

Contact analysis for an anisotropic half-domain with micropatterns considering friction

***Hideo Koguchi¹, Shuma Suzuki², and Masahiro Taroura³**

¹Department of Mechanical Engineering, Nagaoka University of Technology, Japan.

²Graduate School of Nagaoka University of Technology, 1603-1 Kamitomioka, Nagaoka, Niigata, Japan.

³Taiheikogyo Co. Ltd. Tokai, Aichi 476-0003, Japan

*Corresponding author: koguchi@mech.nagaokaut.ac.jp

Abstract

In the present study, a contact problem between a spherical indenter and a half-anisotropic elastic region with a micropattern is solved under normal and tangential forces considering friction. Surface Green's function, the discrete convolution and the fast Fourier transform (DC-FFT) method are used to calculate displacements on a contact area, and the conjugate gradient (CG) method is employed for calculating a contact pressure, the contact area, shear tractions, and a stick-slip region, respectively. The influences of the shape and density (the ratio of the pattern area per a unit area) of the micropattern and of material anisotropy in the substrate on the friction property for the substrate are investigated. In this study, the substrate with circle- and square-micropatterns are used for the analysis. As the result, it is found that the shear traction concentrates at the edges and corners of circle- and square-patterns, respectively. The apparent friction coefficient varies with the direction of the anisotropic principal axis.

Keywords: Contact problem, Anisotropic material, Friction, Micropattern.

Introduction

By machining a micropattern on the surface of material, the friction property on the surface is desired to control as we design. Then, the functional enhancement in various manufacturing processes can be promoted. For example, there are needs to control an inflow and a transformation to the die of the work piece partially by machining a micropattern for a surface of the press die and blank holder. However, we do not yet understand enough the effect of pattern shapes on friction properties or the advantage that give a micropattern. Therefore, the present study investigates the friction property through a contact analysis between a spherical indenter and a half-anisotropic elastic region with the micropattern. In particular, the normal and tangential forces are applied to the surface of the anisotropic and isotropic elastic body, and investigated the relationship between the frictional force and the micropattern. Vlassak et al. (2003) analyzed a contact problem, which the indenter in an arbitrary shape is penetrated in the normal direction for the surface of the anisotropic material. In addition, Lin et al. (2008) analyzed a contact problem of a three-dimensional rough surface, and He et al. (2004) performed a three-dimensional contact analysis of the rough surface with an arbitrary geometry. Cattaneo (1938) and Mindlin (1949) first established mathematical models for analyzing a partial slip problem in an elastic contact. They assumed that the magnitude of shear traction in a contact area could not exceed a static friction limit. Recently, Ciavarella (1998) extended Cattaneo-Mindlin's partial slip model to plane contact problems. However, the contact of dissimilar materials does not obey the classic theory of the Cattaneo-Mindlin model, in which the effects of shear tractions on the normal displacement were not considered. It is difficult to derive an analytical solution for the contact problems with coupled normal and tangential loads. Therefore, Kalker (1977) proposed the method for analysis using the variational principle, instead of solving a contact problem analytically. Moreover, Chen and Wang (2008) proposed a method for analysis in the case considering a partial slip on a three-dimensional contact problem. Dini et al. (2010) conducted a contact analysis to the surface with many hemispherical projections.

In the present paper, a partial slip contact problem on half-anisotropic elastic bodies with a micropattern is analyzed. The conjugate gradient (CG) method, the discrete convolution and the fast Fourier transform (DC-FFT) are used for the contact analysis. Distributions of contact area and contact pressure are calculated using the CG method. The surface displacement for a contact pressure is calculated using the DC-FFT method. Furthermore, the influence coefficient is obtained using a surface Green function in a three-dimensional anisotropic elastic body. As a result, a ratio of the apparent stick-slip area and the friction coefficient of the surface with a micropattern are obtained for various directions of horizontal external force. In addition, the apparent friction coefficient for the surface with patterns is analyzed.

Theory and Descriptions

A model for contact problem between a rigid spherical ball and a surface with a micropattern is shown in Fig. 1. The x - and y -axes are set on the surface, while the z -axis directs towards the substrate. The ball indenter is pressed onto the substrate by a normal load, P_0 , in the z -direction. Tangential loads, F_x and F_y , are applied to the ball in parallel directions to the x - and y - axes. The contact interaction results in a balance between normal pressure p , shear tractions q_x and q_y at the interface. The contact analysis of the semi-infinite isotropic elastic body considering friction was conducted by Mindlin (1949), and the validity of the result was checked in experiment, too. More general contact model is summarized as follows,

$$\begin{Bmatrix} u_x(x,y) \\ u_y(x,y) \\ u_z(x,y) \end{Bmatrix} - \begin{Bmatrix} \delta_x \\ \delta_y \\ \delta_z \end{Bmatrix} = \begin{Bmatrix} s_x(x,y) \\ s_y(x,y) \\ g(x,y) - h_0(x,y) \end{Bmatrix}, \quad (1)$$

where u_x , u_y , and u_z are the surface displacement under external forces in the direction of three axes, δ_x , δ_y , and δ_z are the rigid body displacements, respectively, s_x and s_y the relative slip distance parallel to the x - and y -axes, h_0 is the initial surface gap, and g the surface gap between the indenter and the substrate after loading. The meanings of variables are shown in Fig. 2. Furthermore, the rigid body displacements δ_x , δ_y , and δ_z for isotropic materials are derived from the equations below,

$$\delta_x = \delta_0 \left\{ 1 - \left(1 - F_x / \mu_f P_0 \right)^{2/3} \right\}, \quad \delta_y = \delta_0 \left\{ 1 - \left(1 - F_y / \mu_f P_0 \right)^{2/3} \right\}, \quad (2)$$

$$\delta_z = 9P_0^2 (1 - \nu^2) / 16RE^2, \quad (3)$$

where

$$\delta_0 = 3\mu_f P_0 (2 - \nu)(1 + \nu) / 8aE, \quad (4)$$

a is a radius of the contact area,

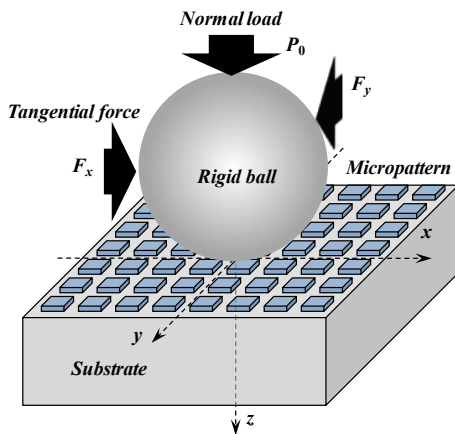


Figure 1. Model of contact analysis

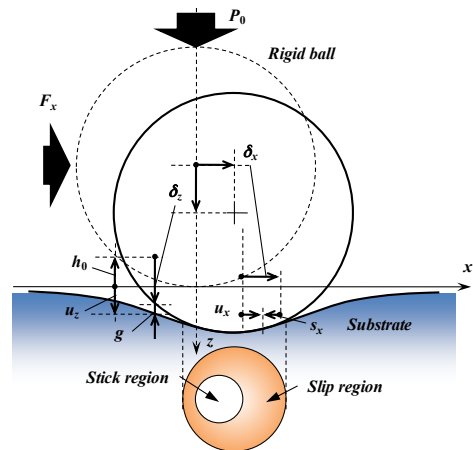


Figure 2. Description of contact situation

$$a = \left\{ 3RP_0(1-\nu^2)/4E \right\}^{1/3}, \quad (5)$$

R is a radius of rigid ball, E is Young's modulus of elastic body, and ν is a Poisson's ratio of elastic body.

In contact analysis, we determined the contact area, pressure and shear traction so as to satisfy the conditions of the following formula using Eq. (1).

Let

$$g(x, y) = h_0(x, y) - \delta_z + u_z(x, y). \quad (6)$$

The contact pressure p is thought as follows,

$$\begin{cases} g(x, y) = 0 : p(x, y) \geq 0 & \text{(In contact)} \\ g(x, y) > 0 : p(x, y) = 0 & \text{(In separation)} \end{cases}, \quad (7)$$

$$\int_{\Omega} p(x, y) dS = P_0, \quad (8)$$

where Ω is the contact area, and P_0 is the normal load.

The shear tractions in the stick and slip regions are assumed to obey the following conditions:

$$\text{In the stick region: } \sqrt{q_x^2(x, y) + q_y^2(x, y)} \leq \mu_f p, \text{ and } \sqrt{s_x^2(x, y) + s_y^2(x, y)} = 0 \quad (9)$$

$$\text{In the slip region: } \sqrt{q_x^2(x, y) + q_y^2(x, y)} = \mu_f p, \text{ and } \sqrt{s_x^2(x, y) + s_y^2(x, y)} \neq 0 \quad (10)$$

$$\int_{\Omega} q_i(x, y) dS = F_i, \quad i = x, y, \quad (11)$$

where the shear tractions q_i is the product of the friction coefficient μ_f and the contact pressure p .

Furthermore, the elastic displacement in the contact region is calculated in order to perform contact analysis. If the force $\mathbf{q} = (q_x, q_y, p)$ is applied to a contact surface, the surface displacement \mathbf{u} is calculated from the following equation,

$$\mathbf{u}(x, y) = \iint_{\Omega} \mathbf{K}(x - x_s, y - y_s) \mathbf{q}(x_s, y_s) dx_s dy_s \quad (12)$$

where (x, y) is an observation point, (x_s, y_s) is a source point of force, \mathbf{K} is the displacement of the observation point when unit concentration load acts to a source point. Generally, \mathbf{K} is expressed in a matrix form. The response function for displacement will be described later. Applying the two-dimensional Fourier transform to Eq.(12) yields $\hat{\mathbf{u}} = \hat{\mathbf{K}} \cdot \hat{\mathbf{q}}$, where the two-dimensional Fourier transform is defined by

$$\hat{f}(\eta_1, \eta_2) = \int_{-\infty}^{\infty} \int_{-\infty}^{\infty} f(x, y) e^{i(\eta_1 x + \eta_2 y)} dx dy \quad (13)$$

Calculation is carried out iteratively so that the normal load P_0 and tangential forces F_x and F_y which are given as a prior condition may satisfy Eqs. (8)-(12). Moreover, the distributions of contact pressure p and shear tractions q_x and q_y in a contact region are calculated. In order to solve the basic equation for a contact problem, the field containing a contact surface is divided by a grid.

Grid intervals of the x - and y - directions are set to Δx and Δy . When the coordinates of an arbitrary grid point on the field are $(i\Delta x, j\Delta y)$, the coordinates of the point are represented as (i, j) . The algorithm for resolving the shear tractions proposed by Wang et al. (2010) is used in this study. This method is used for the repetitive calculation considering the coupling effect of contact pressure and shear traction. Furthermore, the stick-slip region and shear traction of the contact region are determined simultaneously.

In this study, the displacement in the contact area is calculated using the DC-FFT method. The displacement under the shear tractions $q_x(i, j)$ and $q_y(i, j)$ is obtained by the inverse Fourier transform of Eq. (13). Thus,

$$\begin{Bmatrix} u_x(i, j) \\ u_y(i, j) \\ u_z(i, j) \end{Bmatrix} = \text{IFFT} \left\{ \begin{bmatrix} \hat{K}_{q_x}^{u_x}(i, j) & \hat{K}_{q_y}^{u_x}(i, j) & \hat{K}_p^{u_x}(i, j) \\ \hat{K}_{q_x}^{u_y}(i, j) & \hat{K}_{q_y}^{u_y}(i, j) & \hat{K}_p^{u_y}(i, j) \\ \hat{K}_{q_x}^{u_z}(i, j) & \hat{K}_{q_y}^{u_z}(i, j) & \hat{K}_p^{u_z}(i, j) \end{bmatrix} \begin{Bmatrix} \hat{q}_x(i, j) \\ \hat{q}_y(i, j) \\ \hat{p}(i, j) \end{Bmatrix} \right\}, \quad (14)$$

where IFFT denotes the inverse Fourier transform, and $\hat{}$ expresses the Fourier transform of each function. Equating Eq. (14) to the x - and y - component of Eq.(1) yields

$$\text{IFFT} \left\{ \begin{bmatrix} \hat{K}_{q_x}^{u_x}(i, j) & \hat{K}_{q_y}^{u_x}(i, j) & \hat{K}_p^{u_x}(i, j) \\ \hat{K}_{q_x}^{u_y}(i, j) & \hat{K}_{q_y}^{u_y}(i, j) & \hat{K}_p^{u_y}(i, j) \end{bmatrix} \begin{Bmatrix} \hat{q}_x(i, j) \\ \hat{q}_y(i, j) \\ \hat{p}(i, j) \end{Bmatrix} \right\} - \begin{Bmatrix} \delta_x \\ \delta_y \end{Bmatrix} = \begin{Bmatrix} s_x(i, j) \\ s_y(i, j) \end{Bmatrix}, \quad (15)$$

where pressure distribution $p(i, j)$ is provided from the contact problem of only normal load. Then, shear tractions q_x and q_y can be determined from Eq.(15) by using the CG method coupling with constraint conditions (Eqs.(9) and (10)).

Once the shear tractions q_x and q_y are obtained from the above procedure, the displacements u_x for q_x and u_y , respectively, can be determined in terms of the influence coefficients by using the DC-FFT method. Then, the surface vertical gap g is updated by adding the displacements due to the shear tractions. Furthermore, the CG method is also employed to renew the contact pressure, and the new pressure is used for further update of the shear tractions.

Now, we need to derive the influence function for a semi-infinite anisotropic region. We consider that a force $\mathbf{f}=(f_x, f_y, f_z)$ is applied to the coordinate origin. The equilibrium equation for anisotropic materials can be expressed using the displacement, u_i :

$$C_{ijkl}u_{k,lj} = 0. \quad (16)$$

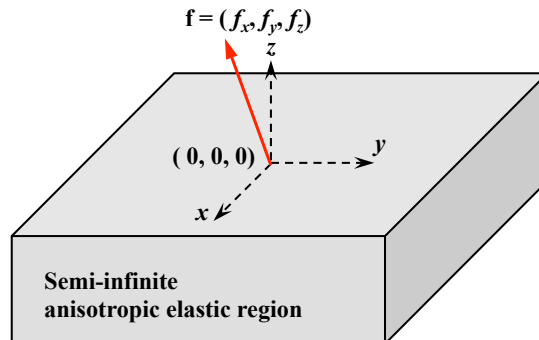


Figure 3. The coordinate system for an influence function

The two-dimensional spatial (x_1 - x_2) Fourier transform is applied to Eq.(16). Then, an ordinary differential equation of displacement is derived. The general solution of the differential equation is assumed to be $\hat{\mathbf{u}} = \mathbf{a}e^{-ip\rho x_3}$. Where p and \mathbf{a} satisfy the following eigenrelation:

$$\{\mathbf{Q} + p(\mathbf{R} + \mathbf{R}^T) + p^2\mathbf{T}\}\mathbf{a} = 0 \quad (17)$$

where $Q_{ik} = C_{ijks}n_jn_s$, $R_{ik} = C_{ijks}n_jm_s$, and $T_{ik} = C_{ijks}m_jm_s$ with $\mathbf{n} = [n_1, n_2, 0] = [\cos\theta, \sin\theta, 0]^T$, $\mathbf{m} = [0, 0, 1]^T$. The angle θ is used in the variables $(\eta_1, \eta_2) = (\rho n_1, \rho n_2)$ of the Fourier transform and taken from the η_1 axis. Finally, the displacement obtained from the inverse Fourier transform is expressed as follows:

$$\mathbf{u}(x_1, x_2, x_3) = \frac{i}{4\pi^2} \int_{-\infty}^{\infty} \int_{-\infty}^{\infty} \frac{1}{\rho} \mathbf{A} \langle e^{-ip_s \rho x_3} \rangle \mathbf{B}^{-1} \mathbf{f} e^{-i(\eta_1 x_1 + \eta_2 x_2)} d\eta_1 d\eta_2 \quad (18)$$

where $\mathbf{A} = [\mathbf{a}_1, \mathbf{a}_2, \mathbf{a}_3]$, $\mathbf{B} = [\mathbf{b}_1, \mathbf{b}_2, \mathbf{b}_3]$, $\langle e^{-ip_s \rho x_3} \rangle = \text{diag}[e^{-ip_1 \rho x_3}, e^{-ip_2 \rho x_3}, e^{-ip_3 \rho x_3}]$, and $\mathbf{b}_j = (\mathbf{R}^T + p_j \mathbf{T}) \mathbf{a}_j$.

Results and Discussions

Result of isotropic material

For a verification of the validity of the result of analysis, the same problem as Wang et al. (2010) is analyzed. The condition for analysis is shown in Table 1(a). The Boussinesq's solution for an isotropic elastic body is used for calculating the response coefficient of traction and pressure. Distributions of the contact pressure and shear tractions are shown in Figs. 4(a) ~ (c). In addition, the contact pressure and shear tractions are normalized by the maximum pressure of Hertz contact theory, $p_H = 860\text{MPa}$, and coordinates are normalized by the contact radius of Hertz contact theory, $a = 0.105\text{mm}$. In this analysis, the displacement in a normal direction to the surface induced by the tangential force that acts on the surface of a half-infinite domain is also taken into consideration. Therefore, the maximum contact pressure causes at the position where the maximum shear traction q_x shown in Fig.4(b) occurs. The distributions of contact pressure and shear traction are agreed with the results of Wang et al. (2010).

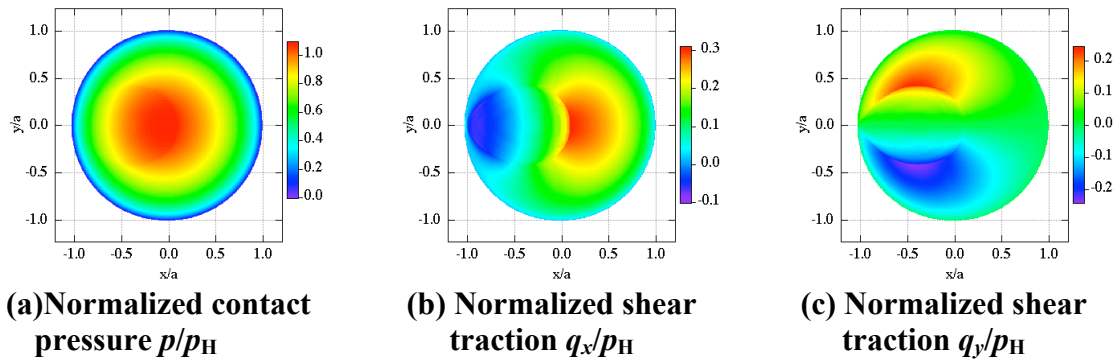


Figure 4. Contour plots of normalized contact pressure and shear tractions by $p_H=860.03\text{MPa}$ and $a=0.10537\text{mm}$

Results of anisotropic material

Distributions of the contact pressure and shear tractions on the plane of Fe(111) are shown in Figs. 5(a)~(c). Moreover, pressure and shear tractions were normalized by the maximum pressure of Hertz contact theory $p_H = 931.62\text{MPa}$, and coordinates were normalized by the contact radius of Hertz contact theory $a = 0.10124\text{mm}$. As compared with the result of isotropic material, the maximum and minimum values of the contact pressure and shear tractions in the anisotropic material are similar to those in the isotropic Fe. However, the shapes of the distribution are different,

but the difference of absolute values of the shear tractions is small. Here, Young's moduli and Poisson's ratio for anisotropic materials Fe(111), Cu(111) and Ni(111) are calculated using $E_{(111)} = 4/(2s_{11} + 2s_{12} + s_4)$ and $\nu_{(111)} = -(s_{11} + 5s_{12} - s_{44}/2) / (3s_{11} + 3s_{12} + 3s_{44}/2)$, respectively, where s_{11} , s_{12} and s_{44} are elastic compliance of materials.

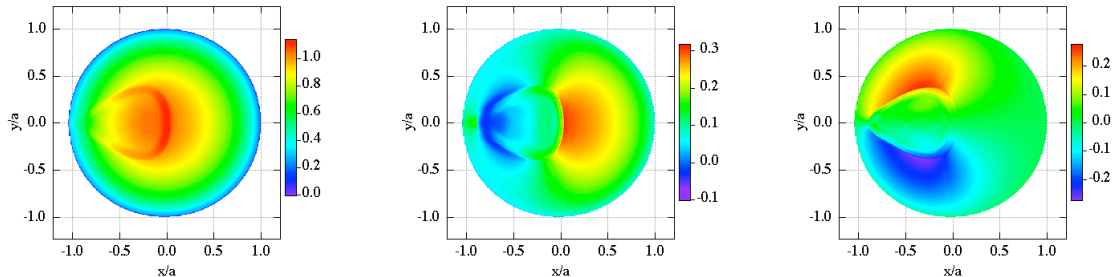
At first, a contact analyze for the surface of Cu (isotropy, anisotropy) and Ni (isotropy, anisotropy) which have four kinds of micropatterns shown in Fig.6 under the condition (c) shown in Table 1 is

Table 1. Condition for analysis

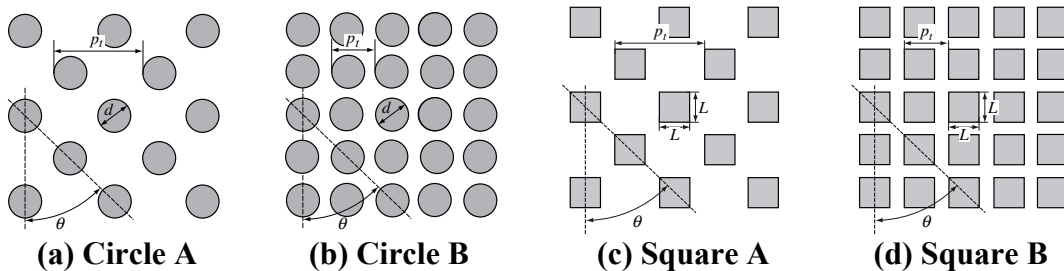
	(a)	(b)	(c)			
Material	Fe(Isotropy)	Fe(111)	Cu(Isotropy)	Ni(Isotropy)	Cu (111)	Ni (111)
Young's modulus E	210 GPa	220.41 GPa	128.73 GPa	220.64 GPa	128.53 GPa	227.34 GPa
Poisson's ratio ν	0.3	0.391	0.345	0.302	0.503	0.423
Number of grid points	512 × 512		256 × 256			
Distance of grid points	0.5 μm		20.0 μm			
Shape	Plane		Circle(ϕ 400 μm), Square(\square 340 μm)			
Pattern			1280 μm, 640 μm			
Pitch	-	-				
Height	-	-	30.0 μm			
Radius of indenter R	18.0 mm		200 mm			
Coefficient of friction μ_f	0.28571		0.3			
Normal load P_0	20 N		6.00 kN			
Tangent force $F_x (= 0.6\mu_f P_0)$	3.43 N		1.08 kN			

Table 2. Material properties used in the analysis (GPa)

	C_{11}	C_{12}	C_{13}	C_{15}	C_{22}	C_{23}	C_{25}	C_{33}	C_{44}	C_{46}	C_{55}	C_{66}
Fe(111)	300.1	111.6	97.26	20.26	300.1	97.26	-20.26	314.4	79.93	-20.26	79.93	94.25
Cu(111)	218.6	103.7	86.51	24.32	218.6	86.51	-24.32	235.8	40.25	-24.32	40.25	57.44
Ni(111)	325.7	129.0	103.2	36.58	325.7	103.20	-36.58	351.6	72.47	-36.58	72.47	98.33



(a) Normalized contact pressure p/p_H (b) Normalized shear traction q_x/p_H (c) Normalized shear traction q_y/p_H
Figure 5. Contour plots of normalized contact pressure and shear tractions by $p_H=931.62\text{MPa}$ and $a=0.10124\text{mm}$



(a) Circle A (b) Circle B (c) Square A (d) Square B
Figure 6. Geometry and size of micropatterns

carried out, and the friction property for different micropatterns is investigated. Elastic constants for the anisotropic material are shown in Table 2. Figure 7 demonstrates the distributions of shear traction, q_x , and the contact pressure p on the surface of Cu(111). In case of Circle A, the shear traction q_x concentrates at the edge of each circle, and a positive shear traction occurs at the right side of the circle like Fig.4(b), since the external force which is applied to the rigid indenter directs in the positive direction of the x -axis. Large shear traction occurs near the center in the whole contact area. In case of Circle B, the shear traction q_x is less than that in Circle A (Fig.7(b)), and the concentration of q_x at the edge reduces moderately. This is attributed to the increase of pattern density. This is caused by the increase of contact area and the decrease of average contact pressure. There is no space to show the results for Squares A and B. Similar results are deduced for square patterns, furthermore, for Ni(111).

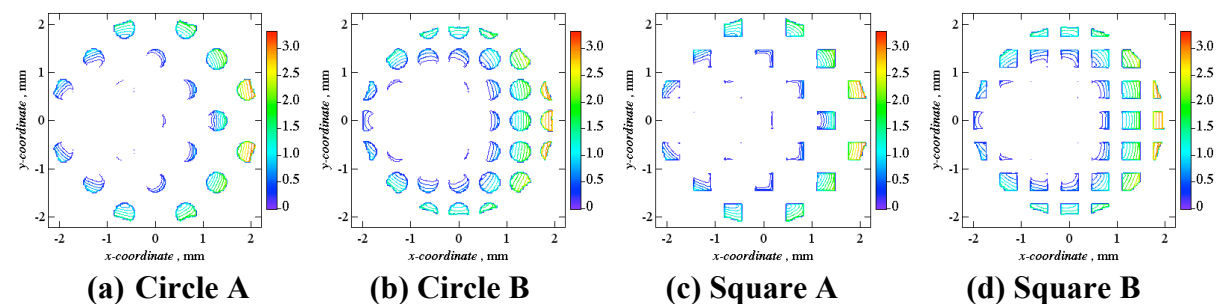
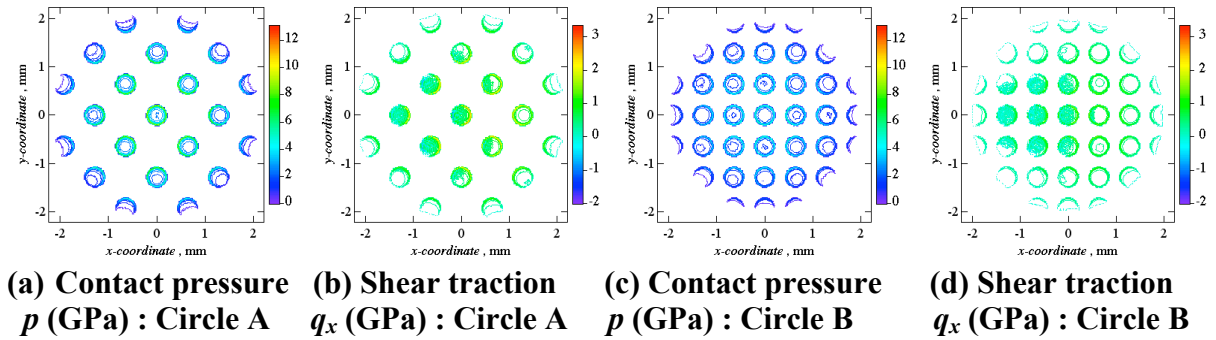
Slip distance and stick region

The maps of slip distance, s_{xy} , for each surface pattern are shown in Fig.8. The stick region indicates the region of $s_{xy}=0$. For Circle A, it is found that the slip distance increases in the direction of the applied force within the region of a lower contact pressure, and the stick region exits at the opposite side of the slip region. Comparing the stick region with the distribution of shear tractions, q_x and q_y , it is found that the shear tractions vary significantly within the stick region. Figure 8(b) shows the map of slip distance for Circle B. It is found that the width of stick region in Circle B is less than that in Circle A. Next, comparing Fig.8(c) with Figs.8(a), (b) and (d), it is found that the stick region for square patterns is similar to that for circular patterns, and the width of stick region decreases with the increase of pattern density. Although the maximum slip distance does not so much vary for all patterns.

Apparent friction coefficient

It is very hard to determine a friction property for each pattern due to the different tendency of the ratio of stick region against the pattern density. Then, a friction coefficient is investigated for the apparent contact area. An analytical solution for contact problem with anisotropic substrate considering friction cannot be available until now. So, the friction coefficient is estimated using the expression for isotropic materials in the study. When material is isotropic, the friction coefficient is obtained from

$$\mu_a = \delta_x a^3 K_E / \{P_0 (a^2 - c^2)\} \quad (19)$$



where $K_E=8E\{3(1+\nu)(2-\nu)\}$, ν is Poisson's ratio, E is Young's modulus for the isotropic substrate. When the substrate is an isotropic flat surface, the friction coefficient calculated using Eq.(19) is 0.3. When material is anisotropic, K_E is composed of anisotropic elastic moduli. We do not know the form until now. The value of K_E is determined from the data of the flat anisotropic substrate for different directions of applied force. The obtained values of K_E are shown in Fig.9(a). In the present analysis, the arrangement and direction of the patterns are fixed, and the direction of applied horizontal force is rotated 15° by 15° until 180° with respect to the z -axis. Then, the influence of pattern on the apparent friction coefficient, μ_a , is investigated. The results are shown in Fig.9(b). It is found that the apparent friction coefficient for the surfaces with patterns is larger than that for the isotropic substrate with the flat surface. It is found that the value of friction coefficient for the surface with high pattern density is less than that with low pattern density. This is due to the increase of contact pressure in low pattern density. The influence of pattern shape on the friction coefficient can be a little observed.

Conclusion

In the present study, a contact problem between a rigid spherical indenter and a half-anisotropic elastic region with the micropattern was analyzed under normal and tangential forces considering friction. Furthermore, the apparent friction property for the surface with a micropattern was investigated. From the results, the following conclusions can be drawn:

- (1) The difference of absolute values of the shear tractions between isotropic material and anisotropic material were not so much large. However, the shapes of the map for shear tractions were different.
- (2) For the surface with the micropattern, the contact pressure concentrated at the edge of each pattern, and the shear tractions also concentrated at the sites corresponding to the contact pressure.
- (3) The apparent friction coefficient for a high density of micropattern was less than that for a low density.

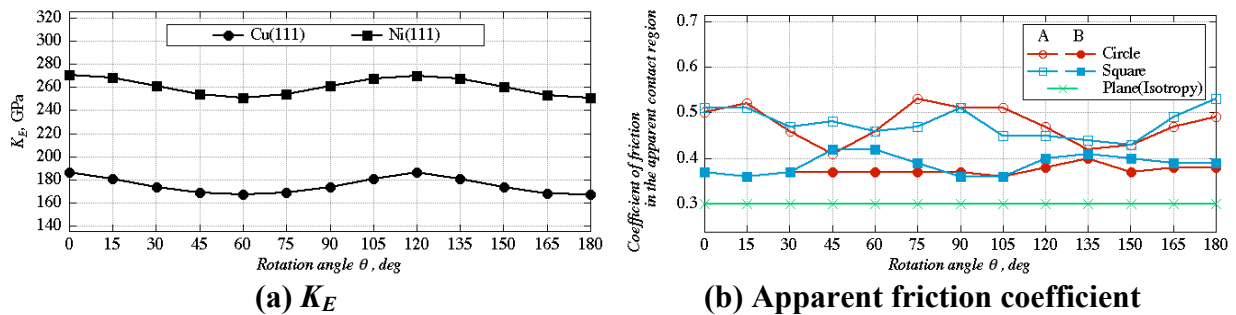


Figure 9. Variation of K_E and apparent friction coefficient

References

- Vlassak, J.J., Ciavarella, M., Barber, J.R., Wang, X., (2003), The indentation modulus of elastically anisotropic materials for indenters of arbitrary shape, *J. Mech. Phys. Solids*, 51, pp.1701–1721.
- Lin Y. and Ovaert T.C., (2008), Three-dimensional rough surface contact model for anisotropic materials, *J. Tribol.*, 130, 021402.
- He L. and Ovaert T.C., (2004), A rough surface contact model for general anisotropic materials, *J. Tribol.*, 126, pp.41–49.
- Cattaneo, C., (1938), Sul Contatto Di Due Corpi Elastici: Distribuzione Locale Degli Sforzi, *Rend. Accad. Naz. Lincei*, 27, pp. 342–348, 474–478, 434–436.
- Mindlin, R. D., (1949), Compliance of Elastic Bodies in Contact, *J. Appl. Mech.*, 16, pp. 259–268.
- Ciavarella, M., (1998), The Generalized Cattaneo Partial Slip Plane Contact Problem. I—Theory, *Int. J. Solids Struct.*, 35(18), pp. 2349–2362.
- Kalker, J. J., (1977), Variational Principles in Contact Elastostatics, *J. Inst. Math. Appl.*, 20, pp. 199–219.
- Chen, W. W., and Wang, Q., (2008), A Numerical Model for the Point Contact of Dissimilar Materials Considering Tangential Tractions, *Mech. Mater.*, 40(11), pp. 936–948.
- Dini, D. Hill, D. A., (2009), Frictional Energy Dissipation in a Rough Hertzian Contact, *J. Tribol.*, 131(2), 021401.
- Wang, Z. J., Wang, W. Z., Wang, H., Zhu, D., and Hu, Y. Z., (2010), Partial Slip Contact Analysis on Three-Dimensional Elastic Layered Half Space, *J. Tribol.*, 132(2), 021403.